Potential-dependent Surface Compression of Gold and its Link to Electrocatalytic Reactivity

Yvonne Gründer, Gary S. Harlow[†], Elizabeth Cocklin, Joshua Fogg, Jack W. Beane and Christopher A. Lucas*

Oliver Lodge Laboratory, Department of Physics, University of Liverpool, Liverpool, L69 7ZE, UK

* Corresponding author: clucas@liv.ac.uk

[†]Current address: Lund University, Department of Physics, Box 118, SE-221 00 Lund, Sweden

Abstract

The surfaces of gold exhibit a rich physical behaviour that is interesting not only from a structural perspective but also for applications in areas such as heterogeneous catalysis and electrocatalysis. In this paper we show that the hexagonal reconstructions of both the Au(111) and the cubic Au(001) surfaces in alkaline electrolyte exhibit a potential-dependent in-plane compression that is remarkably similar despite the substantial difference in the geometry of the underlying substrate. The compressibility is linked to the charge on the surface Au atoms within a simple free electron model. The interplay between surface charge and the adsorption of hydroxide species determines both the surface compression and the reversible lifting of the reconstructions. In the presence of adsorbed carbon monoxide both the potential-induced changes in the surface compression and the lifting of the reconstruction are suppressed leading to the promotion of electrocatalytic reactivity.

Keywords: Surface reconstruction, Gold, Electrochemistry, Electrocatalysis, X-ray diffraction

1. Introduction

The low index surfaces of Au single crystals all exhibit surface reconstruction at room temperature in which the surface atomic layer adopts a different symmetry to the underlying bulk crystal. Whereas the Au(110) surface exhibits a 'missing-row' reconstruction, the Au(001) and Au(111) surfaces both exhibit form hexagonal surface layers with increased atomic density (~20% and 4% respectively compared to the underlying bulk atomic layers). The Au(111) and Au(001) surface reconstructions have been studied by numerous experimental techniques under ultra-high vacuum (UHV) conditions and the Au(111) surface has also been examined by theoretical methods in an effort to understand the link between electronic and surface atomic structure and relate this to functional properties, such as catalytic activity [1,2]. This is particularly challenging due to the large size of the reconstructed surface unit cell and similar calculations for the Au(001) surface have yet to be performed. The renewed interest in the surfaces of Au has been motivated by the discovery by Haruta and co-workers of the enhanced catalytic activity towards the oxidation of carbon monoxide of gold nanoparticles on oxide supports [3,4]. This has stimulated interest in Au for both heterogeneous catalysis and electrocatalytic applications. The surface reconstruction of Au in the electrochemical environment has received particular attention as it is possible to control the surface atomic structure by the applied electrode potential [5-7]. Recently, a rather surprising promoting effect of adsorbed carbon monoxide on the electrooxidation of alcohols by gold catalysts was observed. Rodriguez, Koper and co-workers described the enhanced electrocatalytic properties in a series of papers [8-12] in which they showed that the enhancement effect only occurs on the Au surfaces that exhibit hexagonal reconstruction, i.e., Au(111) and Au(001).

In this paper a detailed study of the structural changes that occur at the interface between the Au(111) and Au(001) electrodes and 0.1 M KOH electrolyte is described. The

aim of the experiments was to explore the dependence of the Au surface reconstructions on the applied electrode potential, particularly at the very negative potentials that can be achieved in alkaline solutions due to the high pH. The experimental methodology involves the use of surface x-ray diffraction (SXRD) to probe with high resolution the potential dependence of the in-plane surface atomic structure. The results indicate that both the Au(111) and Au(001) reconstructed surfaces undergo a potential-dependent surface compression that is remarkably similar, despite the substantial difference in the geometry of the underlying atomic structure. In CO-saturated electrolyte, the presence of CO adsorbed onto the Au surfaces completely suppresses the changes in Au surface compression. This is discussed in relation to the enhancement of electrocatalytic reactivity caused by adsorbed CO on the reconstructed Au surfaces.

2. Experimental Methods

The Au(111) and Au(001) single crystals (miscut< 0.1°) were prepared by sputtering and annealing in a UHV system for several days until sharp LEED patterns were observed. The samples were then removed from UHV and, prior to the x-ray experiments, annealed in a butane flame before cooling in air. The crystal was then transferred to the electrochemical 'thin-layer' x-ray cell with a drop of ultra-pure water protecting the surface and was immersed at open circuit potential in electrolyte. The experimental procedure followed that of similar studies reported previously [7]. Prior to each experiment, the potential was cycled for ~30-60 minutes in the electrolyte solution of 0.1 M KOH over the range -1 V to -0.1 V (at 50 mV/sec) and then held at -1.0 V. This was to ensure reproducible surface preparation ('surface conditioning') in each case [5]. X-ray measurements were performed on beamline BM28 (XMaS) and beamline ID03 at the ESRF, Grenoble and on beamline 7-2 at SSRL, Stanford. The close-packed (111) surface has a hexagonal unit cell that is defined such that

the surface normal is along the $(0, 0, L)_{hex}$ direction and the $(H, 0, 0)_{hex}$ and $(0, K, 0)_{hex}$ vectors lie in the plane of the surface and subtend 60°. The units for H, K and L are $a^*=b^*=4\pi/\sqrt{3}a_{NN}$ and $c^*=2\pi/\sqrt{6}a_{NN}$, where a_{NN} is the nearest-neighbour distance in the crystal (a_{NN} = 2.884 Å). The (001) surface was indexed to the bulk *fcc* unit cell. During the experiment the outer chamber of the x-ray cell was continuously purged with nitrogen to protect the surfaces from oxygen. The reference electrode used in the x-ray cell was Ag/AgCl and all potentials are quoted versus this reference.

3. Results and Discussion

In the UHV environment the clean, low-index surfaces of Au have been shown to reconstruct under certain conditions of sample temperature and surface preparation [13]. In the case of the Au(111) and Au(001) surfaces this leads to the formation of a hexagonal surface layer with a higher atomic density than the underlying bulk crystal. The Au(111) reconstruction involves a small increase in the surface density by compression of the first atomic layer along the <10> direction which leads to a large unit cell, with a $(23x\sqrt{3})$ periodicity [14,15]. Despite its underlying cubic symmetry, the Au(001) surface also exhibits a hexagonal reconstruction of the first atomic layer. This layer is buckled and slightly distorted and the hexagonal structure is aligned close to the [110] bulk direction and is often referred to as a "5x20" or "hex" reconstruction [6,16]. These reconstructions all survive transfer into electrolyte and the nature of the electrode surface structure (reconstructed or unreconstructed) can then be controlled by the application of an electrical potential across the electrode/electrolyte interface [17].

3.1 0.1 M KOH

The Au(001) and Au(111) surfaces have been studied in some detail by SXRD both

under UHV conditions and in the electrochemical environment and the diffraction patterns are well known [18,19]. The Au(001)-hex reconstruction forms two symmetry-equivalent domains (rotated by 90° with respect to each other) that are closely aligned to the underlying bulk lattice. For one of these domains the principal diffraction peak is observed at the (1+δ, 1+δ) in-plane position, where δ~0.2 corresponds to the incommensurability and defines the in-plane lattice constant of the hexagonal overlayer. Thus the in-plane diffraction pattern consists of a hexagon of diffraction spots superimposed onto the square lattice of the underlying cubic Au(001) crystal (see reference [[20]] for a detailed picture). Figure 1 shows the scattered intensity measured along the [1, 1, 0] direction through the (1.2, 1.2, 0.4) reciprocal lattice point at different electrode potentials. The observed peak is due to the surface reconstruction and is present over the potential range -1.0 V to -0.2 V, at more positive potentials the peak is not observed as the reconstruction is lifted. Rocking scans through the diffraction peak showed no rotation of the reconstructed layer with respect to the underlying Au lattice, in agreement with previous studies in alkaline electrolytes [16]. The solid lines in Figure 1 are fits to the measured data with a single Gaussian lineshape and a linear background signal which gives an excellent fit to the data at all potentials.

For the Au(111) surface, the (p x √3) reconstruction gives rise to a well-defined diffraction pattern which, in the surface plane of reciprocal space, is characterized by a hexagon of additional diffraction spots around the scattering that occurs for the bulk Au(111) crystal [5,14,18]. A schematic map of the scattering observed at the (0, 1, 0.5) position is shown in Figure 2. The x-ray measurements for Au(111) that are presented in this paper are representative of a number of experiments that have been performed on different Au(111) crystals over a period of several years. The ordering of the (p x √3) reconstruction and the precise value of p that is obtained after prolonged potential cycling (surface conditioning) can vary from crystal to crystal, however the same effects (reported below) are observed in each

case. The right hand panel of Figure 2 shows data that were measured at the ID03 beamline at the ESRF in Grenoble. Using the Maxipix 2D detector, a series of theta scans along the *l*=0.5 plane around the (0, 1, *l*) crystal truncation rod (CTR) were measured over a range of potentials for the Au(111)/0.1M KOH system. The measured scans were binned using the *BINoculars* software [21] and then combined to create a full image with the pixel coordinate converted to the corresponding (*h*, *k*) value. A typical image is shown in Figure 2 and a movie of the potential dependence of these images is included as Supplementary Information. Figure 3 shows data from another experiment in which the scattered intensity was measured along the [1, 1, 0] direction (the q_r direction shown in Figure 2) through the (0, 1, 0.3) reciprocal lattice point as the potential was scanned from -1.0 V to 0.4 V in small potential steps. In each scan shown, two clear peaks can be seen, the one at q_r=0 corresponding to the scattering from the (0, 1, L) CTR and the peak at q_r~0.038 which arises due to the (p x √3) reconstruction. In these units the stripe separation, p, is given by $p=\sqrt{3}/(2q_r)$, where q_r is the separation from the CTR position (at q_r =0), to the position of the reconstruction peak. For both the Au(001) and Au(111) surfaces it can be seen that the reconstruction peaks show a dependence on the applied electrode potential in the potential region below ~0 V where the surfaces are reconstructed.

Measurements, such as those shown in Figures 1 and 3, were made as the potential was stepped positively from -1.0 V. From the fits to the data the integrated intensities of the reconstruction peaks, the in-plane Au near-neighbour spacing, a_{NN}, and the coherent domain size, L, can be obtained [5] and are shown in Figures 4 and 5 for the Au(001) and Au(111) surfaces respectively. In Figures 4(a) and 5(a) the red symbols also show the corresponding potential dependence of the integrated intensities of the scattering measured at the bulk CTR positions, i.e. (1, 1, 0.4) for Au(001) and (0, 1, 0.3) for Au(111). The intensities at these two positions closely follows the trends shown by the reconstruction peaks in each case up to the

point where the reconstruction begins to lift. For both Au(111) and Au(001) lifting of the reconstruction causes the intensity at the CTR positions to rise (at -0.3 V for Au(001) and +0.2 V for Au(111)) as the intensity of the scattering at these positions is larger for the (1x1) termination of the crystal surfaces than for the reconstructed surfaces. What is clear from Figures 4 and 5 is that there is a rich behavior in the potential dependence of the surface reconstructions across the potential regions in which they are stable. Before discussing the results it is important to make a note of the reproducibility of the data shown with respect to the rotated domains that are present both on Au(111) and Au(001). In the case of Au(001), symmetry-equivalent reflections also give the same results indicating that in this case the change in the Au near-neighbour spacing is isotropic. For Au(111) we have made measurements on four different samples and although the p value of the (p x √3) reconstruction measured at -1.0 V after potential cycling can be different (varying from 23.5-26), similar potential-dependent results to those shown in Figure 5 for the compression of the reconstruction atomic layer were obtained, i.e. the data in Figure 5 is representative. In the case of Au(111), the value of a_{NN}, shown in Figure 5, corresponds to the near-neighbour spacing along the p direction of the reconstruction, as the reconstruction is uniaxially incommensurate.

The differences between the behavior of the Au surfaces in UHV and under electrochemical conditions can be accounted for in terms of (i) the presence of co-adsorbed solvent and adsorbed species, and (ii) differing surface potentials (and continuously adjustable) variations in electrode potential. The former effect communally results in the formation of an adsorbed layer of water, the adsorption of hydrogen, reversible/irreversible formation of oxygenated species and the adsorption of anions from supporting electrolyte. The latter effect results in potential-induced changes of the surface electron density. We discuss the results in terms of two potential regions determined by the electrochemistry

[22,23]. For potentials E<-0.45 V, there is no specific adsorption onto the Au surfaces. E=-0.45 V correlates with the onset of the adsorption of hydroxide species, OH^-. Interestingly it has also been postulated, based on differential capacitance measurements [24], that this potential corresponds to the potential of zero charge (*pzc*). In the potential region -1.0 V<E<-0.45 V it can be seen that the reconstructions both on the Au(111) and Au(001) surfaces show remarkably similar behavior. In particular the intensities of the reconstruction peaks increase as the potential is increased positively from the negative limit. This increase is correlated to an increase in the in-plane correlation length, L, of the reconstructed phase and a concomitant decrease in the near neighbour spacing, a_{NN}, i.e. an in-plane surface compression. The increase of the in-plane Au-Au spacing at negative potential can be understood as a pure charging effect; in the absence of specific adsorption the excess surface charge determines the Au-Au surface interaction independent of the underlying Au substrate. Similar electrocompressibility has been observed in halide anion adlayers with hexagonal geometry adsorbed onto noble metal surfaces [25-27] and for underpotentially deposited metal adlayers on metal surfaces [28-30]. The 2D isothermal compressibility of the reconstructed monolayer is $\kappa_{2D}=\frac{1}{N_{ion}e}\left(\frac{dA}{dE}\right)$ with $\left(\frac{dA}{dE}\right)$ the change in area A per adsorbate atom [31], which can be deduced from the experimentally obtained data. The applied potential is E and N_{ion} is the ionic charge of the surface atom. The exact charge of the surface atoms is unknown. Assuming a 2D free electron gas model the electrocompressibility κ_T can be deduced [32,33] to be $\kappa_T=\frac{m_e A^2}{\pi \hbar (Z-N_{ion})^2}$ where $(Z-N_{ion})$ denotes the number of electrons contributing to the free electron gas, m_e is the electron mass and ħ is Planck's constant h/(2π). In the case of gold, Z=1 for the 6s electron and N_{ion} gives the modification through the additional charge of the surface atom. Obtaining $\left(\frac{dA}{dE}\right)$ and the surface area, A per atom from the experimental value for nearest neighbour distance, a_{NN}, the charge of the surface gold atoms $e \cdot N_{ion}$ can

be obtained by assuming a 2D isothermal compressibility for the electrocompressibility ($\kappa_{2D} = \kappa_T$) and is shown in Figure 6 as a function of the applied potential. With these values an electrocompressibility of the order of 1Å^2/eV is obtained which is of the same order as the values found for electrochemically deposited metal monolayers [28,30,34]. Though the model assumed is based on the free electron model and neglects any possible influence of the 5d electrons, it shows that the change in electrocompressibility observed can be explained through a change in the charge of the surface atoms. The minimal nearest neighbour distance corresponds in this case to the point where the charge on the surface atom changes sign.

At -0.45 V both the Au(111) and Au(001) surface exhibit reconstructions that are closest to the phases observed under UHV conditions. The potential of E=-0.45 V marks the onset of hydroxide adsorption onto the Au surfaces and leads to the lifting of the surface reconstructions. In the case of the Au(111) surface, however, the initial stage of lifting results in the formation of a stable intermediate phase (-0.2 V<E<0 V) prior to the complete lifting of the reconstruction. Similar intermediate phases prior to the lifting of the reconstruction have also been observed in acidic electrolyte solution by STM [35]. In their study of hydroxide adsorption onto Au(111), Chen and Lipkowski [22] proposed that OH^- forms a polar bond at negative potential, the polarity of which decreases at positive charge densities due to strong screening of the anion charge by the charge on the metal or by significant charge transfer from OH^- to Au. As has been shown explicitly in recent studies of halide adsorption onto Cu(001) electrode surfaces [36,37], the sub-surface metal layers play a key role in the bonding mechanism. It is clear that the Au(111) surface is able to accommodate significant OH^- adsorption by a change in the in-plane compression (or p value). Recent density functional theory (DFT) calculations have shown that there are only small energy differences in the formation of these reconstructed phases [38]. In contrast, the reconstruction on the Au(001) surface immediately begins to lift as the potential increases above -0.45 V and

there is no change in the Au-Au surface compression. In this case it appears that the adsorption of hydroxide species drives the lifting of the reconstruction [39,40].

3.2 0.1 M KOH saturated with carbon monoxide

The potential-dependent changes in the Au surface structure are interesting from a fundamental perspective, however, an additional key question is whether the structure changes are linked to electrocatalytic behaviour. To gain insight into the mechanism behind the promotion of electrocatalytic reactivity by the adsorption of CO, we performed experiments in which the 0.1 M KOH electrolyte was exchanged to a CO-saturated 0.1 M KOH electrolyte with the potential held at the negative limit, followed by measurements analogous to those shown in Figures 1 and 3. Representative results are shown in Figure 7 for both Au(001) and Au(111). In CO-saturated solution at -1.0 V, both the Au(001) and Au(111) surfaces exhibit the reconstructed phase with an in-plane lattice constant near to the maximum surface compression, i.e a_{NN}~2.76 Å, with no significant change in the in-plane correlation length, L, compared to that observed in CO-free electrolyte. Furthermore upon potential steps over the range -1.0 V to -0.2 V no change in the surface compression was observed on either surface and there was also negligible change in the integrated intensities of the reconstruction peaks (data measured at -1.0 V and -0.5 V are shown in Figure 7). It is thus apparent that adsorbed CO suppresses the potential-induced changes in the Au near neighbour lattice spacing. No electrocompression is observed and thus the simple model of a 2D electron gas fails as a description, possibly due to a modification of the electron density of the surface atoms through a bonding to the CO and/or a possible hybridisation of the 6s electrons. It is likely that the adsorbed CO molecule accommodates the changes in the surface charge (thus acting as a tuneable dipole) rather than the Au surface atoms. This may be the origin of the enhanced electrocatalytic activity in that the reactions no longer require a through-gold

interaction and take place in the outer layer of the electrochemical double layer structure at the interface. This is consistent with the model of CO-promoted OH^- adsorption as the mechanism for the enhanced electrooxidation of alcohols on the hexagonal Au surfaces that are unique to the Au(111) and Au(001) single crystals. As has been previously shown [23], adsorbed CO also stabilizes the Au(001) reconstructed phase over a much larger potential range. Figure 8 shows the potential dependence of the intensity measured at (0, 0, 1.02), an 'anti-Bragg' position on the specular CTR which is sensitive to the atomic density of the Au surface atomic layer and hence shows large changes when the reconstruction is lifted and formed. The results demonstrate that the Au(001) reconstruction is preserved in the presence of CO right up to the onset of oxide formation at positive potentials. In fact the lifting of the reconstructions on both the Au(111) and Au(001) surfaces occurs at similar potentials in CO-saturated electrolyte, i.e. after or concurrent with oxidation of the adsorbed CO.

4. Conclusions

In this paper we have shown that the hexagonal reconstructions that occur on the Au(111) and Au(001) surfaces in the electrochemical environment both exhibit a potential dependent compressibility in alkaline solution. The origin of the compressibility is explained as a pure charging effect at potentials negative of -0.5 V with the highest Au compression observed at -0.5 V. Analysis of the data within a free electron model suggests that the compression is driven by the charge on the surface Au atoms which reaches a minimum at -0.5 V. This potential also marks the onset of the adsorption of hydroxide species, OH^-, which on Au(111) again leads to a reduction in the surface compression and on Au(001) marks the onset of the lifting of the reconstructed phase. In CO-saturated electrolyte, in which CO is adsorbed onto the surface at -1.0 V, the surface compressibility is suppressed and both the Au(111) and Au(001) surface are locked into the highly compressed phases observed at -0.5

V in the CO-free electrolyte. This suggests that the adsorbed CO is able to accommodate the excess surface charge induced by the applied potential and this is the mechanism that underpins the enhancement in electrocatalytic reactivity and the increased stability of the reconstructed surfaces over a larger potential range.

Acknowledgments

GSH, EC, JF and JB acknowledge the support of EPSRC studentships. YG acknowledges the financial support of the Royal Society (UK) through a University Research Fellowship. SXRD measurements were performed on the EPSRC-funded XMaS CRG beamline (BM28) at the ESRF, Grenoble, France, beamline ID03 at the ESRF, Grenoble and beamline 7-2 at SSRL, Stanford. We thank the XMaS beamline team for support of BM28, Francesco Carla for support of ID03 and Nenad Markovic (Argonne National Laboratory) for his contribution to the experiments on beamline 7-2 at SSRL.

Supporting Information

See Supplemental Material at <url> for a movie of the reciprocal space images showing the potential dependence of the Au(111) reconstruction peaks.

Competing Interests

The authors declare that there are no competing interests.

References

[1] F. Hanke and J. Björk, Physical Review B - Condensed Matter and Materials Physics **87**, 235422 (2013).
[2] A. P. Seitsonen, Surface Science **643**, 150 (2016).
[3] M. Haruta, Nature **437**, 1098 (2005).
[4] M. Haruta, T. Kobayashi, H. Sano, and M. Yamada, Chem. Lett **16**, 405 (1987).
[5] J. Wang, B. M. Ocko, A. J. Davenport, and H. S. Isaacs, Physical Review B **46**, 10321 (1992).
[6] B. M. Ocko, J. Wang, A. Davenport, and H. Isaacs, Physical Review Letters **65**, 1466 (1990).
[7] C. A. Lucas and N. M. Markovic, in *Encyclopedia of Electrochemistry: Interfacial Kinetics and Mass Transport*, edited by A. J. Bard, M. Stratmann, and E. J. Calvo (Wiley VCH, Weinheim, 2004), pp. 295.
[8] P. Rodriguez, J. M. Feliu, and M. T. M. Koper, Electrochemistry Communications **11**, 1105 (2009).
[9] P. Rodriguez, Y. Kwon, and M. T. M. Koper, Nature Chemistry **4**, 177 (2012).
[10] P. Rodriguez, N. Garcia-Araez, and M. T. M. Koper, Physical Chemistry Chemical Physics **12**, 9373 (2010).
[11] P. Rodriguez, N. Garcia-Araez, A. Koverga, S. Frank, and M. T. M. Koper, Langmuir **26**, 12425 (2010).
[12] P. Rodríguez, A. A. Koverga, and M. T. M. Koper, Angewandte Chemie - International Edition **49**, 1241 (2010).
[13] P. A. Thiel and P. J. Estrup, *The Handbook of Surface Imaging and Visualization* (CRC Press: Boca Raton, 1995).
[14] J. Wang, A. J. Davenport, H. S. Isaacs, and B. M. Ocko, Science **255**, 1416 (1992).
[15] I. M. Tidswell, N. M. Marković, and P. N. Ross, Surface Science **317**, 241 (1994).
[16] I. M. Tidswell, N. M. Marković, C. A. Lucas, and P. N. Ross, Physical Review B **47**, 16542 (1993).
[17] D. M. Kolb and J. Schneider, Electrochim.Acta **31**, 929 (1986).
[18] A. R. Sandy, S. G. J. Mochrie, D. M. Zehner, K. G. Huang, and D. Gibbs, Phys.Rev.B **43**, 4667 (1991).
[19] D. L. Abernathy, D. Gibbs, G. Grübel, K. G. Huang, S. G. J. Mochrie, A. R. Sandy, and D. M. Zehner, Surf.Sci. **283**, 260 (1993).
[20] D. Gibbs, B. M. Ocko, D. M. Zehner, and S. G. J. Mochrie, Phys.Rev.B **42**, 7330 (1990).
[21] S. Roobol, W. Onderwaater, J. Drnec, R. Felici, and J. Frenken, J. Appl. Crystallog. **48**, 1324 (2015).
[22] A. Chen and J. Lipkowski, Journal of Physical Chemistry B **103**, 682 (1999).
[23] M. E. Gallagher, B. B. Blizanac, C. A. Lucas, P. N. Ross, and N. M. Marković, Surface Science **582**, 215 (2005).
[24] S. B. Aoun, Z. Dursun, T. Koga, G. S. Bang, T. Sotomura, and I. Taniguchi, Journal of Electroanalytical Chemistry **567**, 175 (2004).
[25] C. A. Lucas, N. M. Markovic, and P. N. Ross, Phys.Rev.B **55**, 7964 (1997).
[26] O. M. Magnussen, Chemical Reviews **102**, 679 (2002).
[27] B. M. Ocko, O. M. Magnussen, J. X. Wang, and T. Wandlowski, Physical Review B - Condensed Matter and Materials Physics **53**, R7654 (1996).
[28] O. R. Melroy, M. F. Toney, G. L. Borges, M. G. Samant, J. B. Kortright, P. N. Ross, and L. Blum, Journal of Electroanalytical Chemistry **258**, 403 (1989).
[29] M. F. Toney, J. G. Gordon, and O. R. Melroy, in *X Rays in Materials Analysis II:*

Novel Applications and Recent Developments (Publ by Int Soc for Optical Engineering, Bellingham, WA, United States
San Diego, CA, USA, 1991), pp. 140.
[30] M. F. Toney, J. G. Gordon, M. G. Samant, G. L. Borges, O. R. Melroy, D. Yee, and L. B. Sorensen, Physical Review B **45**, 9362 (1992).
[31] J. G. Dash, in *Films on Solid Surfaces*, edited by J. G. Dash (Academic Press, 1975), pp. 145.
[32] C. Kittel, *Introduction to Solid State Physics* 1996).
[33] N. W. Ashcroft and N. D. Mermin, *Solid State Physics* (Holt, Rinehart and Winston, New York, 1976).
[34] O. R. Melroy, M. F. Toney, G. L. Borges, M. G. Samant, J. B. Kortright, P. N. Ross, and L. Blum, Physical Review B **38**, 10962 (1988).
[35] C. Vaz-Domínguez, A. Aranzábal, and A. Cuesta, The Journal of Physical Chemistry Letters **1**, 2059 (2010).
[36] Y. Grunder and C. A. Lucas, Physical Chemistry Chemical Physics **19**, 8416 (2017).
[37] Y. Joly *et al.*, Journal of Chemical Theory and Computation (2017).
[38] E. Torres and G. A. DiLabio, J. Phys. Chem. C **118**, 15624 (2014).
[39] K. P. Bohnen and D. M. Kolb, Surf.Sci. **407**, L629 (1998).
[40] S. Venkatachalam, P. Kaghazchi, L. A. Kibler, D. M. Kolb, and T. Jacob, Chemical Physics Letters **455**, 47 (2008).

Figure Captions

Figure 1. In plane x-ray diffraction from the reconstructed Au(001) electrode surface in 0.1 M KOH electrolyte, measured along the [1, 1, 0] direction through the reconstruction peak at ~(1.2, 1.2, 0.4) measured at an electrode potential **(a)** -1.0 V **(b)** -0.5 V and **(c)** -0.2 V (versus Ag/AgCl). The data is fitted with a Gaussian lineshape (solid line). The dashed vertical line indicates the peak position measured at -0.5 V.

Figure 2. (left) A schematic of the scattering in the surface plane of reciprocal space around the (0, 1, 0.5) CTR position (solid symbol) indicating the peaks that arise due to the (p x √3) reconstruction (open symbols) and the direction (q_r) of the scans shown in Figure 3 of the manuscript. **(right)** A contour map of the measured x-ray intensity in the l=0.5 plane around the (0, 1, l) CTR. Each of the reflections brought about by the reconstruction are outlined by a white circle and correspond to reflections from the 3 rotated domains of the reconstruction. A movie of the potential dependence of this contour map is included as supplementary information.

Figure 3. In plane x-ray diffraction from the Au(111) electrode surface in 0.1 M KOH electrolyte, measured along the [1, 1, 0] direction through the (0, 1, 0.3) CTR position at **(a)** 0.4 V **(b)** -0.15 V **(c)** -0.5 V and **(d)** -1.0 V (versus Ag/AgCl). The data is fitted with a double Lorentzian lineshape (solid line). The dashed vertical lines indicate the peak positions measured at -0.5 V.

Figure 4. (a) Integrated intensity of the reconstruction peak shown in Figure 1 as a function of the applied electrode potential. The red symbols (triangles) correspond to the integrated intensity measured at the CTR position, (1, 1, 0.4). **(b)** Near neighbour, in-plane lattice

constant, a_{NN}, of the Au(001)-hex reconstruction derived from fits to the data such as that shown in Figure 1. **(c)** Domain size of the Au(001)-hex reconstruction.

Figure 5. (a) Integrated intensity of the reconstruction peak shown in Figure 2 as a function of the applied electrode potential. The red symbols (triangles) correspond to the integrated intensity measured at the CTR position, (0, 1, 0.3). **(b)** Near neighbour, in-plane lattice constant, a_{NN}, of the Au(111)-(p x √3) reconstruction derived from fits to the data such as that shown in Figure 2. **(c)** Domain size of the (p x √3) reconstruction.

Figure 6. The potential dependent surface charge per atom obtained for the reconstructed Au(001) and Au(111) surfaces by comparing the experimental electrocompressibility to the compressibility for a 2D layer in the free electron model.

Figure 7. (left) In plane x-ray diffraction from the reconstructed Au(001) electrode surface in 0.1 M KOH electrolyte, measured along the [1, 1, 0] direction through the reconstruction peak at ~(1.2, 1.2, 0.4) measured at an electrode potential **(a)** -1.0 V **(b)** -0.5 V. **(right)** In plane x-ray diffraction from the Au(111) electrode surface in 0.1 M KOH electrolyte, measured along the [1, 1, 0] direction through the (0, 1, 0.3) CTR position at **(c)** -1.0 V **(d)** -0.5 V. The dashed vertical lines are guides for the eye.

Figure 8. The intensity measured at (0, 0, 1.02), an 'anti-Bragg' position on the specular CTR, as the potential is swept (sweep rate = 2 mV/s). Results were obtained in 0.1 M KOH (black symbols) and after saturation of the electrolyte with CO (red symbols).

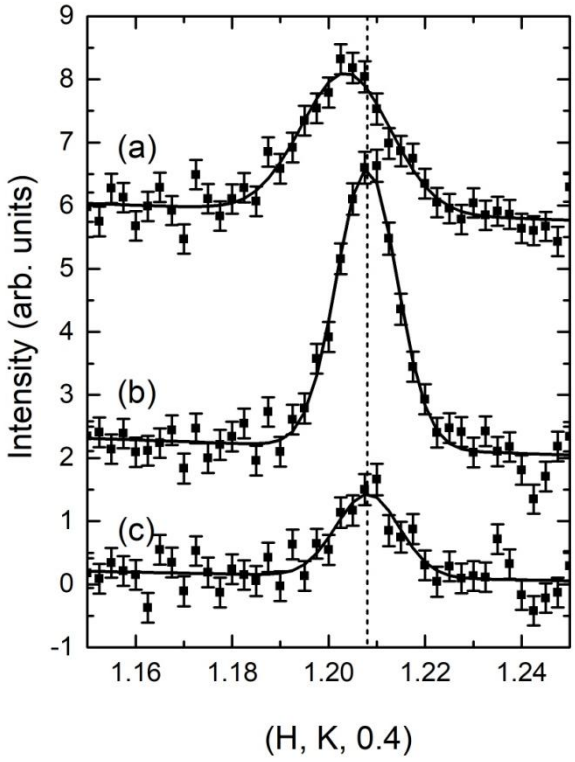
Intensity (arb. units)
(a)
(b)
(c)
9
8
7
6
5
4
3
2
1
0
-1
1.16
1.18
1.20
1.22
1.24
(H, K, 0.4)

Figure 1

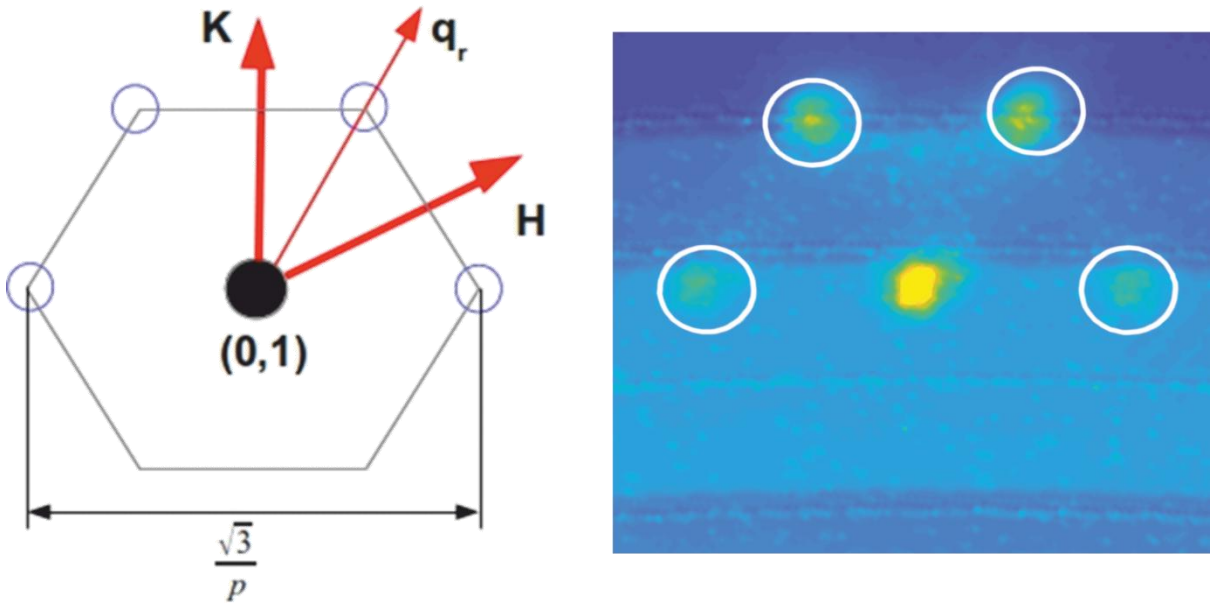

Figure 2

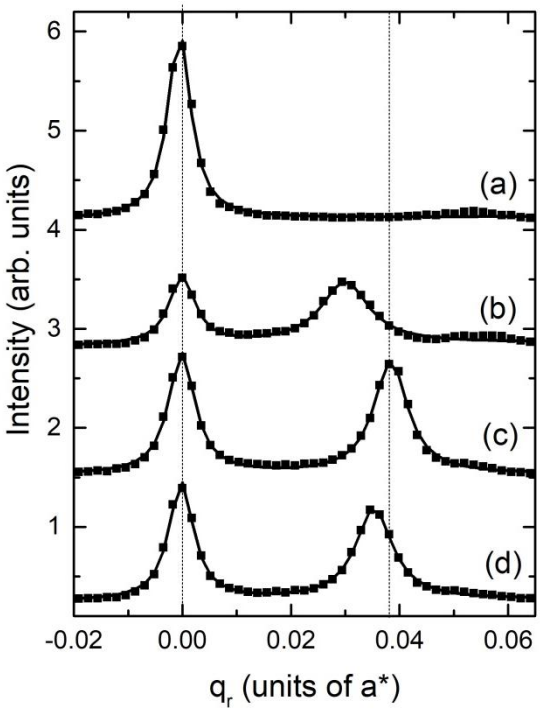
Intensity (arb. units)
6
5
4
3
2
1
(a)
(b)
(c)
(d)
-0.02
0.00
0.02
0.04
0.06
q_r (units of a*)

Figure 3

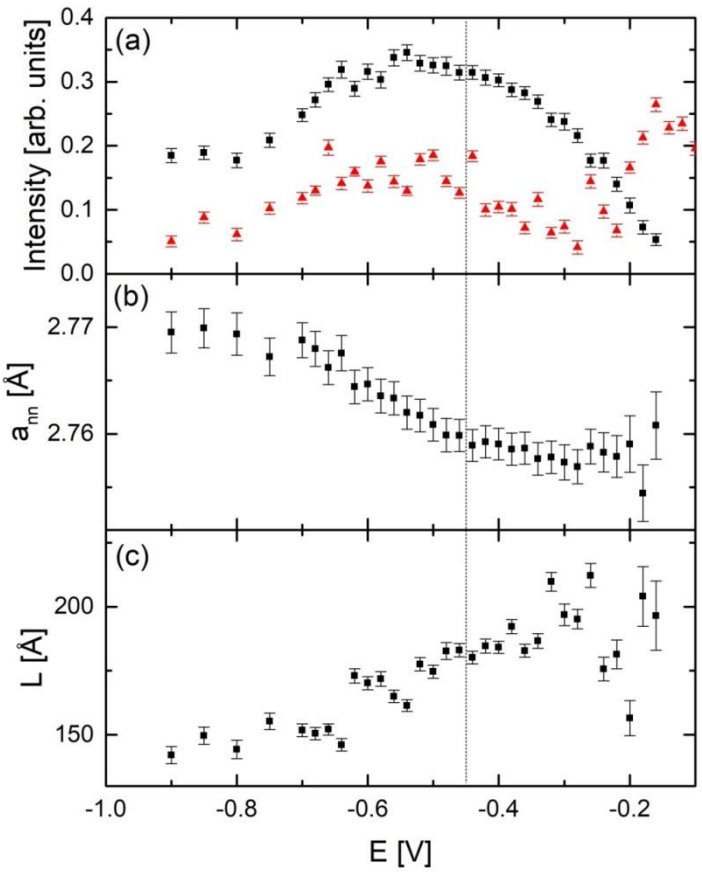
(a)
Intensity [arb. units]
0.4
0.3
0.2
0.1
0.0
(b)
a_{nn} [Å]
2.77
2.76
(c)
L [Å]
200
150
-1.0
-0.8
-0.6
-0.4
-0.2
E [V]

Figure 4

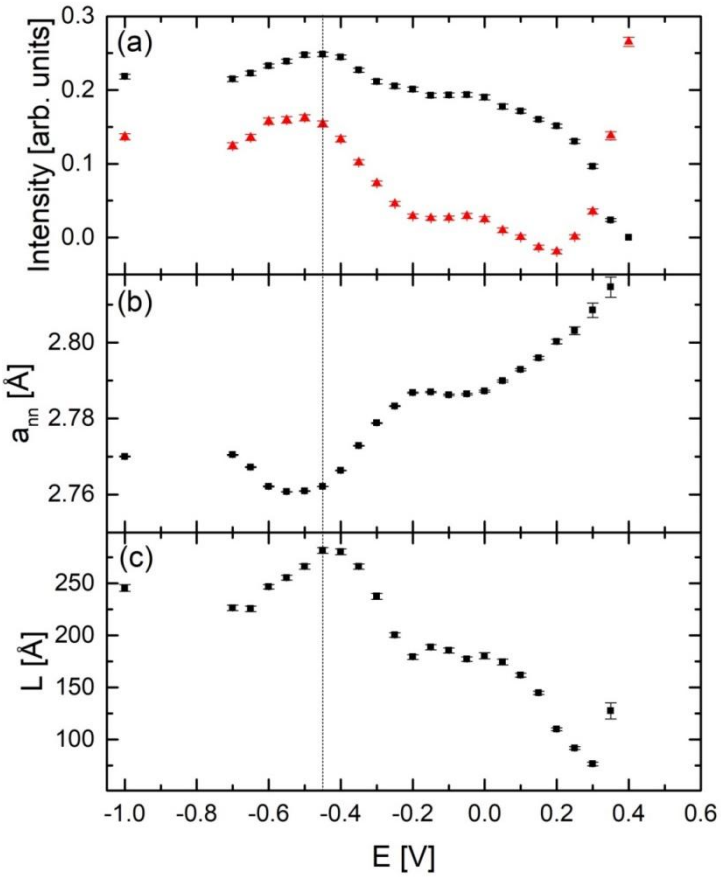
(a)
Intensity [arb. units]
0.3
0.2
0.1
0.0
(b)
a_{mn} [Å]
2.80
2.78
2.76
(c)
L [Å]
250
200
150
100
-1.0
-0.8
-0.6
-0.4
-0.2
0.0
0.2
0.4
0.6
E [V]

Figure 5

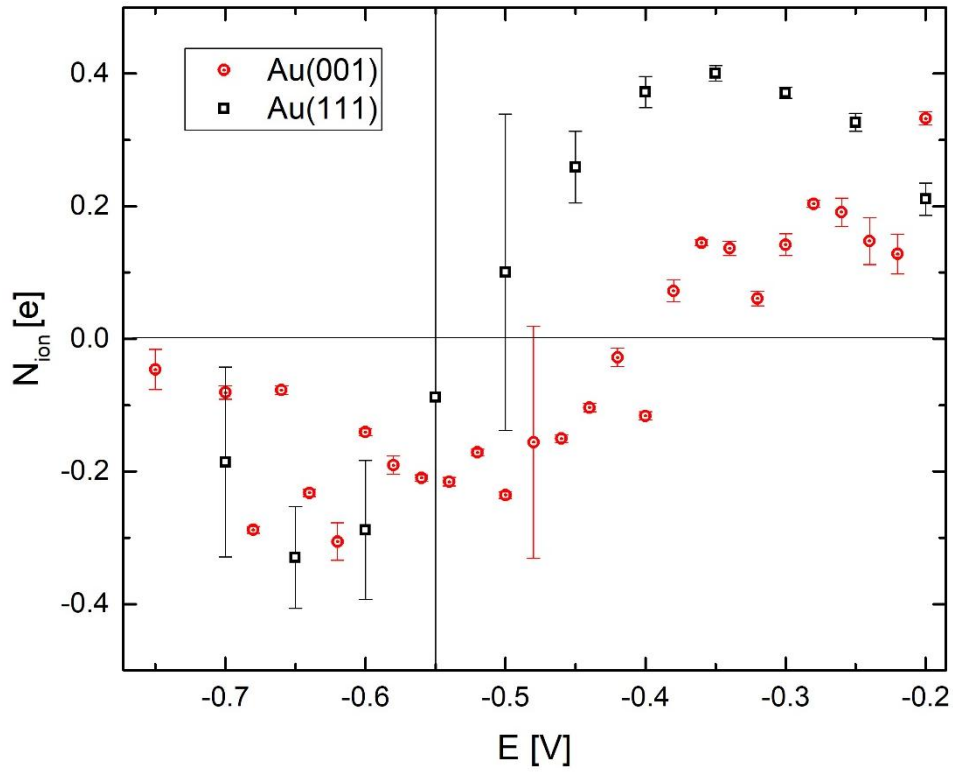

Figure 6

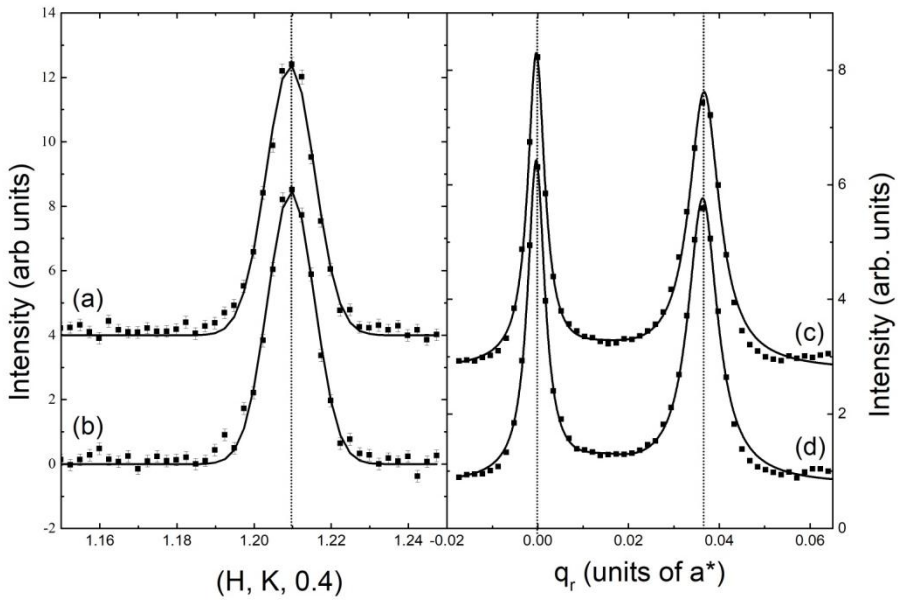
Intensity (arb units)
(a)
(b)
(H, K, 0.4)
Intensity (arb. units)
(c)
(d)
q_r (units of a*)

Figure 7

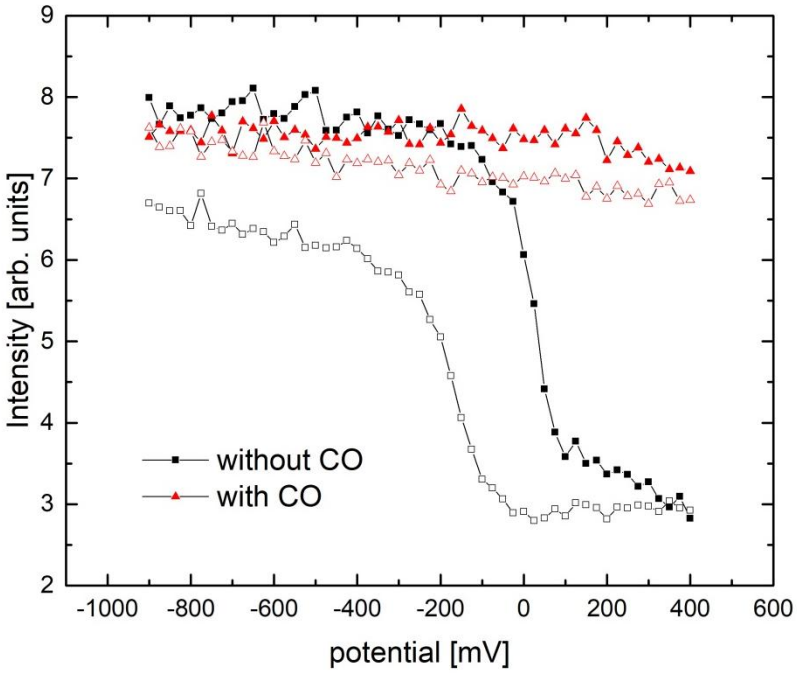
Intensity [arb. units]
potential [mV]
without CO
with CO
9
8
7
6
5
4
3
2
-1000
-800
-600
-400
-200
0
200
400
600

Figure 8